Design and Verification of a GaN-Based, Single Stage, Grid-Connected Three-Phase PV Inverter

Orkhan Karimzada, *Member, IEEE*, and Giulio De Donato, *Senior Member, IEEE*

***Abstract*—This research presents the development of a three-phase GaN-based photovoltaic (PV) inverter, focusing on the feasibility, reliability, and efficiency of gallium nitride (GaN) technology in solar applications. The study systematically explores the use of GaN field-effect transistors (FETs), particularly in enhancing the efficiency and power density of PV systems. A promising inverter topology was identified and extensively analyzed through comprehensive experiments and design optimizations, resulting in a prototype that achieved a remarkable peak efficiency of 96%. Key aspects of the research included performance benchmarking of GaN FETs, design and testing of *LCL* filters for grid connection, PCB design considerations for 3-phase inverters, and thorough evaluation of the inverter's performance in terms of power losses, efficiency, and thermal capability. The successful construction and testing of the inverter prototype, despite laboratory constraints, not only demonstrates the viability of GaN over traditional silicon-based inverters but also significantly contributes to advancing renewable energy technologies, paving the way for more efficient and sustainable power systems.**

***Index Terms*—Gallium nitride (GaN), grid-connection, half-bridge, inverter, journal, *LCL* filter.**

I. Introduction

THE quest for sustainable and efficient energy sources has become paramount in addressing global energy challenges in recent years. Solar power stands out for its ubiquity and potential among renewable energy sources. However, the efficiency and cost-effectiveness of solar energy conversion have been persistent hurdles, limiting its widespread adoption. At the heart of solar energy systems lies the photovoltaic (PV) inverter, a critical component that converts the variable direct current (dc) output of a solar panel into a utility frequency alternating current (ac) that can be fed into a commercial electrical grid or used by a local, off-grid electrical network.

Traditional silicon (Si)-based inverters have dominated the market for years, but their limitations in efficiency, size, and thermal management have led researchers to explore alternative materials. Gallium nitride (GaN), a wide bandgap semiconductor, has emerged as a promising candidate to overcome these limitations. GaN technology is renowned for its higher efficiency, smaller size, and lower heat dissipation compared to Si, making it an ideal choice for PV inverter applications. Additionally, studies have been conducted on the reliability and long-term operation of GaN-based inverter systems, showing promising results, though further extensive testing is still needed to fully establish their reliability compared to proven Si-based inverters [1].

This article focuses on the development and evaluation of a three-phase GaN-based PV inverter, contributing significantly to the field by showcasing the advantages of GaN technology in real-world applications. The primary objective is to investigate the feasibility, efficiency, and reliability of GaN technology in PV inverters. A key contribution of this article is the comprehensive study that includes the design, optimization, and experimental testing of a GaN-based inverter prototype. Specific contributions include performance benchmarking of GaN field-effect transistors (FETs), the design of an optimized *LCL* filter for grid-connected applications, PCB design for three-phase inverters, and the evaluation of the inverter's performance in terms of power losses, efficiency, and thermal management.

The culmination of this research is a prototype that demonstrates the tangible advantages of GaN technology in solar inverters, achieving an impressive peak efficiency of 96%. The findings validate the practical viability of GaN FETs in solar applications, marking a significant step forward in the advancement of renewable energy technologies. This article aims to contribute to the growing body of knowledge in PV inverter technology, offering valuable insights and directions for future research and development in this field.

II. PV Inverter Considerations

The recent surge in the development and application of three-phase inverters across various sectors such as distributed power generation, smart grids, energy storage systems, and electric vehicle charging stations underscores these systems' critical role in modern power quality and control. The versatility of pulsewidth modulation (PWM) techniques, including space vector PWM (SVPWM) and carrier-based SPWM, enables the achievement of variable voltages and frequencies, essential for optimizing the performance of these power systems [2].

A notable advancement in this field is the adoption of GaN high electron mobility transistors (HEMTs), which have

Received 4 July 2024; revised 16 October 2024; accepted 27 November 2024. Date of publication 4 December 2024; date of current version 28 January 2025. Recommended for publication by Associate Editor L. Chang. *(Corresponding author: Orkhan Karimzada.)*

Orkhan Karimzada is with the School of IT and Engineering, ADA University, Baku 1008, Azerbaijan (e-mail: okarimzada@ada.edu.az).

Giulio De Donato is with the Department of Astronautical, Electrical and Energy Engineering (DIAEE), Sapienza-University of Rome, 00161 Roma RM, Italy (e-mail: giulio.dedonato@uniroma1.it).

Color versions of one or more figures in this article are available at https://doi.org/10.1109/TPEL.2024.3511270.

Digital Object Identifier 10.1109/TPEL.2024.3511270

TABLE I
COMPARISON OF PROPERTIES OF GAN, 4H-SIC, AND SI

Properties	GaN	4H-SiC	Si
Bandgap, E_g (eV)	3.39	3.26	1.12
Breakdown field, E_{bm} (MV/cm)	3.3	2.2	0.23
Saturated drift velocity, V_s (10^7 cm/s)	2.5	2.0	1.0
Electron mobility, μ_n (cm^2/V·s)	2000	650	1500
Thermal conductivity, σ (W/cm·K)	1.3	1.5	3.80

demonstrated superior performance over traditional Si insulated gate bipolar transistors (IGBTs) due to their higher switching frequencies. The integration of GaN HEMTs in three-phase inverters has not been extensively studied. In contrast, some research highlighting single-phase inverters with their efficiency in producing clean switching waveforms, achieving high efficiencies, and facilitating a three-phase-leg design featuring GaN transistors achieved a remarkable 97% efficiency, demonstrating the potential of GaN technology in power electronics [3].

Existing studies mainly cover motor control applications and investigations into high-frequency PWM applications have shown significant benefits in terms of motor efficiency, control response, and reduction in torque ripple, indicating the suitability of GaN modules for variable frequency drives (VFDs) and adjustable speed drives (ASDs) [4], [5]. The development of innovative inverter designs, such as the integrated modular motor drive (IMMD) and the exploration of GaN FETs in low-voltage applications, signifies continuous improvements in power density and efficiency [6], [7]. Experimental studies further validate the thermal and switching behavior of GaN devices, underscoring their advantage in the design of ultralow-inductance power cells and in enhancing inverter efficiency under various operational conditions [8], [9].

Despite the promising attributes of GaN-based inverters, challenges such as their sensitivity to external noise due to lower threshold and gate driver voltage requirements persist [10]. Nonetheless, the overarching benefits of GaN technology, including higher switching frequencies, improved efficiency, and compact system design, establish it as a formidable choice for power electronic applications.

The studies reveal significant progress in the utilization of GaN-based three-phase inverters, driven by their enhanced performance, efficiency, and compactness. Future research should aim to address the existing challenges and further explore the capabilities of GaN devices to advance the performance and reliability of three-phase inverters. The collective findings underscore the transformative impact of GaN technology on the power electronics landscape, promising to usher in more efficient, reliable, and compact power conversion systems for a wide array of applications.

III. WHY GAN?

Incorporating GaN semiconductors into PV inverter designs is increasingly recognized due to their superior electrical properties compared to Si and silicon carbide (SiC). As shown in Table I GaN devices, with their higher bandgap energies, enable operation at elevated temperatures and frequencies, facilitating the development of power devices with higher breakdown voltages and smaller die sizes. This results in enhanced efficiency and power density for PV inverters. A notable advancement in GaN technology is the introduction of enhancement-mode (e-mode) high electron mobility transistors (HEMTs), which are typically off without gate voltage, improving power conversion safety and efficiency [11], [12].

The comparison between GaN, Si, and SiC highlights GaN's superior electrical breakdown field and thermal conductivity, which are crucial for reducing losses in PV inverters. These advantages are depicted in [13], showing GaN's lower on-resistance and higher efficiency, underscoring its potential to improve inverter performance significantly.

Transitioning to GaN technology, however, presents challenges such as high switching speeds that can induce parasitic ringing and electromagnetic interference (EMI). Addressing these issues requires careful design considerations, including the adoption of high-frequency magnetics and advanced EMI reduction techniques. GaN devices also introduce unique characteristics like reverse conduction capabilities and the need for specialized gate drive designs, necessitating a thorough understanding to leverage their benefits in PV applications [14], [15], [16].

GaN and SiC can operate at greater temperatures because of their significantly higher bandgap energies. Power devices with higher breakdown voltage can be made because GaN has the highest electrical breakdown field. At a given breakdown voltage, the die of power devices may therefore be smaller. GaN devices are anticipated to be able to switch at greater frequencies than their Si counterparts since the drift velocity of GaN is more than twice that of Si.

Calculating the best theoretical performance that could be attained in each of these contenders provides a more accurate way to compare the performance of devices using these fundamental crystal parameters. Each candidate's theoretical on-resistance can be estimated as

$$R_{\text{on,sp}} = \frac{4V_{\text{br}}^2}{\mu_n \varepsilon_s E_{\text{bm}}^3}$$

where E_{bm} is the electric breakdown field, μ_n is the electron mobility, ε_s is the dielectric constant, and V_{br} is the required breakdown voltage. The theoretical limit of GaN is at least three orders of magnitude lower than that of Si. This equation can be represented as illustrated in Fig. 1.

GaN technology is poised to substantially enhance grid-connected PV inverters' efficiency and power density. Overcoming the limitations of traditional Si and SiC semiconductors, GaN devices pave the way for developing more efficient, compact, and cost-effective solar energy solutions. The integration of GaN devices into PV inverters marks a significant advancement, promising improved efficiency and reliability in renewable energy systems [17], [18].

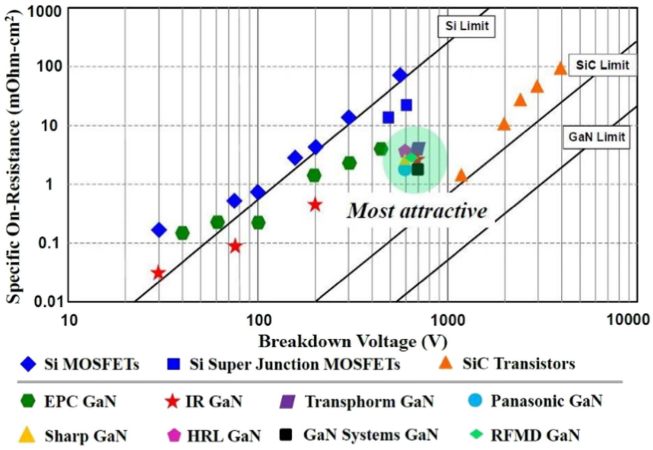

Fig. 1. On-resistance versus breakdown voltage comparison of Si, SiC, and GaN [13].

IV. LCL Filter Design

Electric power systems are progressively using distributed and renewable generation (DG). In the era of smart grids, the safe, dependable, and seamless integration of DG resources is a major driving factor [19], [20], [21], [22], [23]. DC–AC inverters have significantly increased as DG resource usage has increased. The lowest active power losses and best dependability can be achieved while converting dc voltages to ac voltages. On the other hand, a significant number of harmonics are produced as a result of the use of PWM techniques in inverters for switching, which can be extremely hazardous to the equipment in power systems and must be stopped from entering the grid. In order to reduce harmonics fed into the grid and to mitigate output current ripple, high-order filters are typically used as the interface between the grid and inverters. First-order simple *L*-filters were initially presented for this purpose; however, they had poor harmonic attenuation, poor dynamic performance, a larger voltage drop across the filter, and a bulky design [24]. These drawbacks are drastically reduced by using higher order filters in place of traditional *L* filters. Due to its superior performance, *LCL* is the most often used high-order filter for grid-connected power inverters [25].

In the condition that each phase voltage of the inverter and grid is symmetric and *LCL* filters are balanced, three-phase systems could be transformed equivalently into single-phase systems. Fig. 2 shows a single-phase *LCL* filter configuration with internal resistance filter inductors. Here, grid impedance is neglected and assumed to be part of the grid side inductor.

Several characteristics must be considered in designing an *LCL* filter, such as current ripple, inductors ratio, frequency ratio, and damping. The reactive power requirements may cause a resonance of the capacitor interacting with the grid. Therefore, passive or active damping must be added. The common way of adding passive damping is adding a resistor in series with the filter capacitor, which is also implemented in this design. The filter design's most relevant system transfer functions can be directly derived from an impedance analysis of the derived

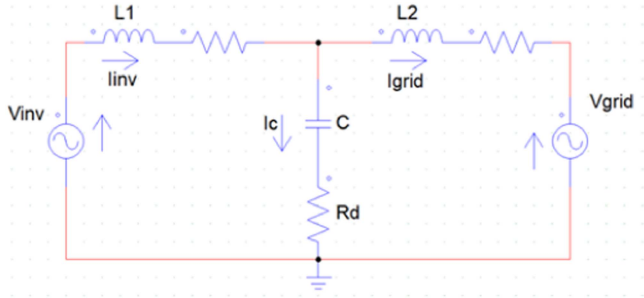

Fig. 2. Single-phase equivalent circuit of *LCL* filter.

equivalent circuit Fig. 2

$$Y(s) = \frac{I_{\text{inv}}(s)}{V_{\text{inv}}(s)} = \frac{1}{sL} \cdot \frac{s^2 + 2\gamma_f \omega_f s + \omega_f^2}{s^2 + 2\gamma_0 \omega_0 s + \omega_0^2} \tag{1}$$

$$Y_c(s) = \frac{I_c(s)}{V_{\text{inv}}(s)} = \frac{1}{L} \cdot \frac{s}{s^2 + 2\gamma_0 \omega_0 s + \omega_0^2} \tag{2}$$

$$Y_f(s) = \frac{I_{\text{inv}}(s)}{V_g(s)} = \frac{1}{s(L + L_f + L_g)} \cdot \frac{2\gamma_0 \omega_0 s + \omega_0^2}{s^2 + 2\gamma_0 \omega_0 s + \omega_0^2} \tag{3}$$

where the parameters are defined as

$$\gamma_f = \frac{\omega_f R_f C_f}{2}, \qquad \omega_f^2 = \frac{1}{C_f(L_f + L_g)}$$

$$\gamma_0 = \frac{\omega_0 R_f C_f}{2}, \qquad \omega_0^2 = \frac{1}{C_f L(L_f + L_g)}.$$

The admittance Y(s) links the voltage applied by the converter to the generated converter side current. This transfer function plays a key role in the closed-loop current control, affecting its performance and system stability. The admittance Yc(s) allows determining the current flowing into the capacitor branch, enabling the filter capacitor. Finally, Yf(s) is the actual filter admittance relating the high-frequency voltage components generated by the converter with the current harmonics injected into the grid. This transfer function determines the frequency-dependent filter attenuation and is thus essential for the *LCL* filter design. A qualitative representation of magnitude Bode plots of Y(s), Yc(S), and Yf(s) is provided in (3), where the effect of different damping resistance values is illustrated.

Since the main controller parameter in this work is grid-side current the Yf(s) transfer function will be considered and analyzed in the remaining part of the thesis. A transfer function of the *LCL* filter with and without damping resistor for grid-side current over inverter output voltage Vg is given in (6)

$$S(s) = \frac{1}{L_1 C_f L_2 s^3 + C_f(L_1 + L_2) R_f s^2 + (L_1 + L_2)s} \tag{4}$$

$$H(s) = \frac{C_f R_f s + 1}{L_1 C_f L_2 s^3 + C_f(L_1 + L_2) R_f s^2 + (L_1 + L_2)s}. \tag{5}$$

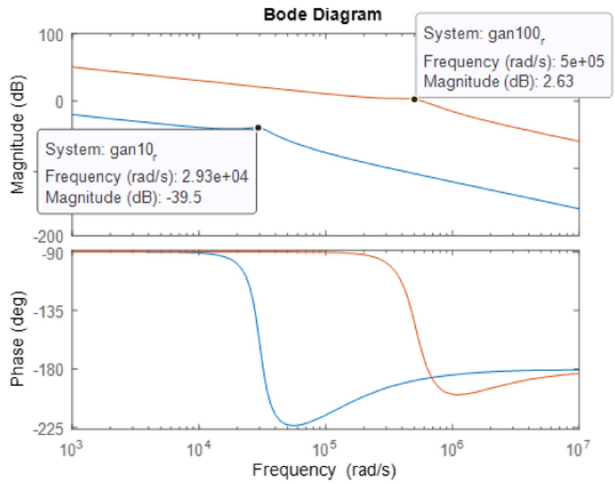

Fig. 3. Bode plot of 100 kHz *LCL* filter.

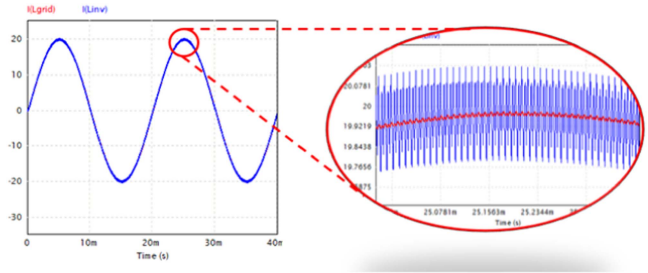

Fig. 4. Current ripple.

The simplified procedure of designing the *LCL* filter is followed. The design steps will be shown in detail below. Bode plot of the 100 kHz *LCL* filter with and without damping resistor are shown in Fig 3. Series resistance with the capacitor effectively eliminated the gain of the plant's resonance frequency

By effectively attenuating harmonic distortions and enhancing grid compatibility, well-designed *LCL* filters contribute significantly to grid-connected PV systems' overall performance and reliability. It is clear from the literature review that there are various methods to calculate *LCL* filter components.

The used simplified method in this work offers a universal solution, perfectly aligning with all grid requirements and meeting diverse filtering expectations. The designed filter is validated through simulation and expected attenuation; current ripple is achieved. The value of inverter side ripple is shown in Fig. 4 for the 100 kHz filters, respectively.

V. Inverter Design and Prototyping

Designed a 3-phase grid-connected inverter consisting of two PCB boards: a control board and a power board. Control board (see Fig. 5) consists of all measurements, protection, and communication circuits. All boards are designed from scratch, developed, and tested in the lab environment in different connecting configurations, like grid connection and load connection.

The control board is designed as a two-layer PCB and has both software and hardware protections. When the DC voltage of the phase current goes out of predefined limits, the microcontroller sends a fault signal. The fault signal is sent to the logic gate, which can send the signal to the power board (see Fig. 5) to disable PWM. In the current version of the inverter, there is no enabled signal connection between the control and power board, but if needed, it can be added easily externally.

Based on the comparison table and relevant considerations, the GS66516B-TR transistor from GaN systems stands out as an excellent choice for the application. It offers several advantages over other devices, such as the lowest gate charge (14 nC), low Rds ON (25 mΩ), and notably low input capacitance (518 pF). These characteristics are crucial for enhancing the overall efficiency and speed of switching, which is vital in power electronics applications like PV systems. Additionally, it has a high continuous current rating of 34 A, meeting the demands of high-power designs.

Although the GS66516B-TR is priced higher than some alternatives, the price per unit decreases significantly when ordered in larger quantities (e.g., over 1000 units). The selection of a 650 V device aligns perfectly with the design requirements for the targeted PV system capacity, making the GS66516B-TR a well-balanced option in terms of performance and long-term cost efficiency.

In the case of GaN switches, the gate signal has to be very clean to avoid unexpected turn-on/off events. In high-frequency applications, there is a high probability that PWM gating signals will get noise from conventional contactors or PCB layouts. One of the best solutions in such an application is optical fiber transmission of PWM signals. Besides better immunity from electromagnetic interference, the optical fiber connection also has excellent resistance to adverse weather conditions, which is also very important in the case of PV inverters. Our inverter design uses an HFBR-0500ETZ Series fiber optic connector from Broadcom. The connectors are designed for various communication speed options, and the current design uses the 1 MBd interface circuit.

The voltages and currents of Phase A (first leg), Phase B (second leg), and the dc input will be measured, these values are measured for controlling the system, they are analog signals that will be sent to the DSP through the analogue to digital conversion (ADC) pins. This adapting stage is needed to allow communication and the interface between the DSP and the power stage since the ADC pins can handle a voltage range from 0 to 3 V, while output from the measurement tools can exceed these limits. Before explaining the design of the adapting stage, the sensors should be explained to get the measurement values of the voltages and currents, as the sensor's output is the signal that will enter the adapting stage. Voltage transducer LV 25/P [26] and current transducer LA 55-P/SP1m [27] are used to measure the voltage and the current, both sensors are hall effect sensors. The sensors are based on a current transformer which means that the output of both of them is a current, the signal that will enter the adapting stage is the voltage across the Rm. The design was made to have equal output voltage at the secondary side

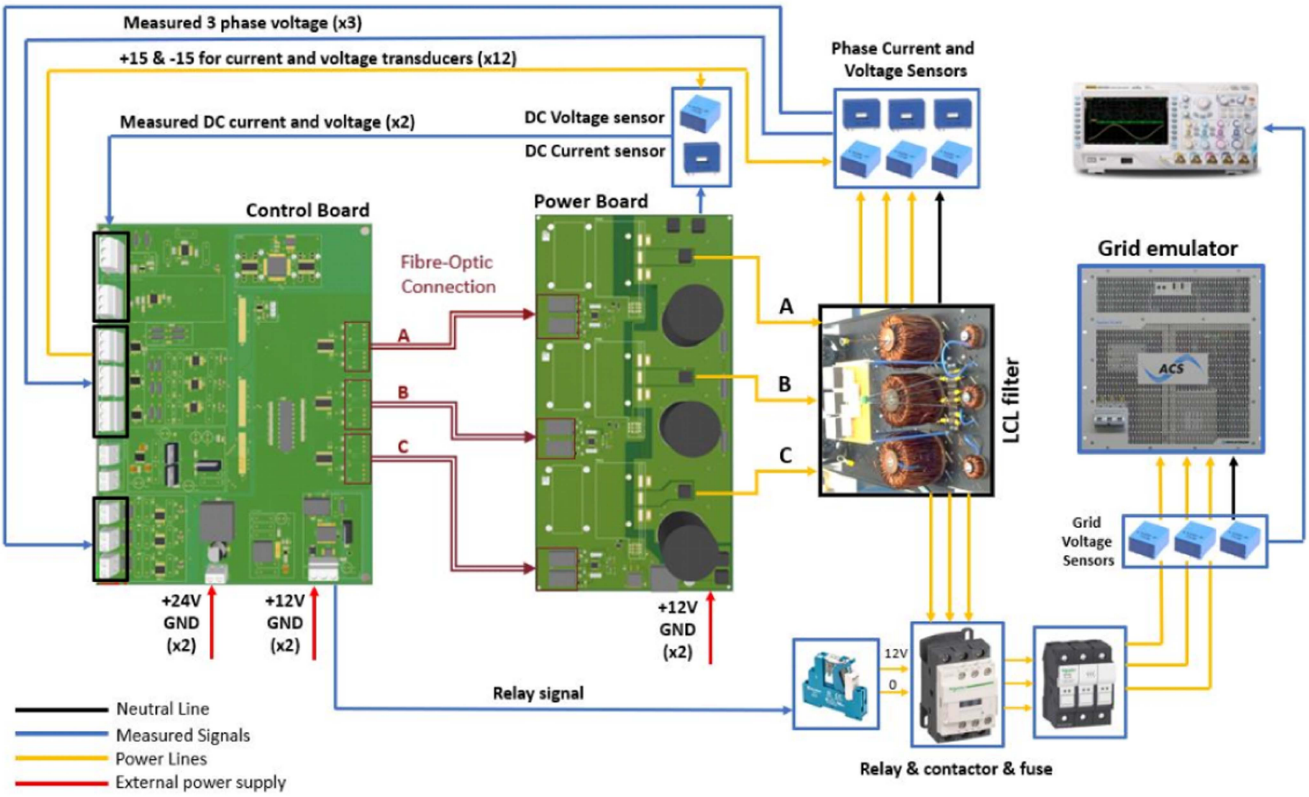

Fig. 5. PCB design of control board.

(1.5 V) from both sensors, so, in this case, one adapting stage design will be required.

To design a three-phase current-controlled SVPWM inverter in rotating synchronous coordinate *d–q* to connect the PV array to the grid. The control scheme is a PI current regulator that regulates the d and q current components. The gain parameter of the regulator is obtained by trial and error. The result gives a unity power factor with low total harmonic distortion (THD). A feed-forward compensation is added to the current loop, which gives a good dynamic and better performance in a steady state. The advantage of this type of control is that the design and assessment of the loop of the current control are practical and simple.

The principle is to convert the abc reference frame of the current into a *d–q* two-phase rotating frame to achieve the rotating frame control structure. By changing the reference frame, the three-phase symmetric grid voltage and grid current become dc variables. The current loop can obtain no steady-state error. The results obtained with this method show that the output current and voltage were of the same phase with a power factor of unity.

VI. Experimental Results

The designed three-phase inverter underwent comprehensive testing under various conditions to evaluate its performance thoroughly and validate the design. Initial tests involved carefully characterizing the *LCL* filter, followed by rigorous evaluation with a pure resistive load to assess its stability and functionality. The performance of the inverter during grid connection was subjected to detailed analysis, aiming to ensure seamless integration with the power grid while maintaining high efficiency and power quality. These grid-connection tests provided valuable insights into the inverter's ability to synchronize with the grid and deliver power consistently and reliably. In addition to performance assessments, extensive thermal analyses were conducted to assess the inverter's heat dissipation capabilities and overall thermal management. Volumetric and gravimetric analyses were conducted further to gauge the inverter's compactness and weight efficiency. These analyses provided critical information on the inverter's physical dimensions and weight, which are important factors for practical applications, particularly in space-constrained installations.

The comparison of system components at two different operating frequencies, 100 and 10 kHz, showcases significant improvements across several physical parameters. Fig. 6 illustrates the comparison of two filter prototypes. At the higher frequency of 100 kHz, the component size is substantially reduced, measuring 215 by 221 mm, compared to the larger dimensions of 281 by 256 mm at 10 kHz, yielding a 54% reduction in size. This size optimization is also reflected in the weight, where the component at 100 kHz weighs only 3.2 kg, a notable decrease from the 7.4 kg at the lower frequency, resulting in a 57% improvement. Similarly, the volume shows a significant contraction, with the higher frequency component occupying just 6115 cubic mm, compared to the 2851 cubic mm at 10 kHz, which equates to

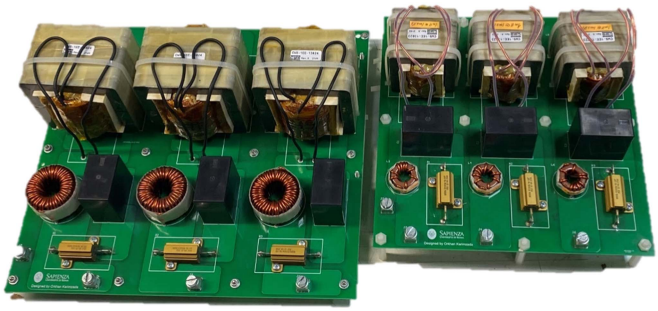

Fig. 6. *LCL* filters mounted on designed PCB.

TABLE II
COMPARISON OF SYSTEM COMPONENTS AT 100 KHZ AND 10 KHZ FREQUENCIES

	100 kHz	10 kHz	Improvement
Size (mm)	215x221	281x256	54%
Weight (kg)	3.2	7.4	57%
Volume (sm^3)	6115	2851	57%

a 57% reduction in volume. These improvements highlight the efficiency and design advantages achieved by operating at higher frequencies, with marked benefits in terms of space-saving, weight reduction, and potentially improved performance in applications where compactness and lighter weight are essential. It is also observed that by increasing the switching frequency, the cost of *LCL* filter can be reduced by 24%. The comparison also shows the advantage of GaN in terms of cost; however, it should be noted that the cost analysis is done based on a single inductor cost. The total cost might be relatively lower by mass ordering the filter component. The comparison table is shown in Table II.

A. Operation Under Grid Connection

As mentioned in previous sections, the experimental setups consist of the control board, power board, auxiliary circuits and some protection equipment, as shown schematically in shows a picture of the experimental setup connected to the grid emulator (Fig. 7).

For the grid synchronization tests REGATRON TC.ACS grid emulator is used, which represents the newest generation of fully programmable, full 4-quadrant grid simulation systems. Intuitive application-based software allows for manual operation, programming, and automated test runs. A set of predefined voltage shapes—sine, clipped sine, sine divers, square, multifunctional ramp, triangle, sawtooth, and user-definable slope—facilitates a quick and easy definition of specific grid situations. The software also offers data 213 acquisition, storage, and documentation throughout the system.

As mentioned before, the inverter is tested with two filters—one is for the 10 kHz switching frequency and another is for 100 kHz. Since both filters are designed using the same design procedure and the results are identical except for resonance frequencies, only 100 kHz filter, experimental results are presented

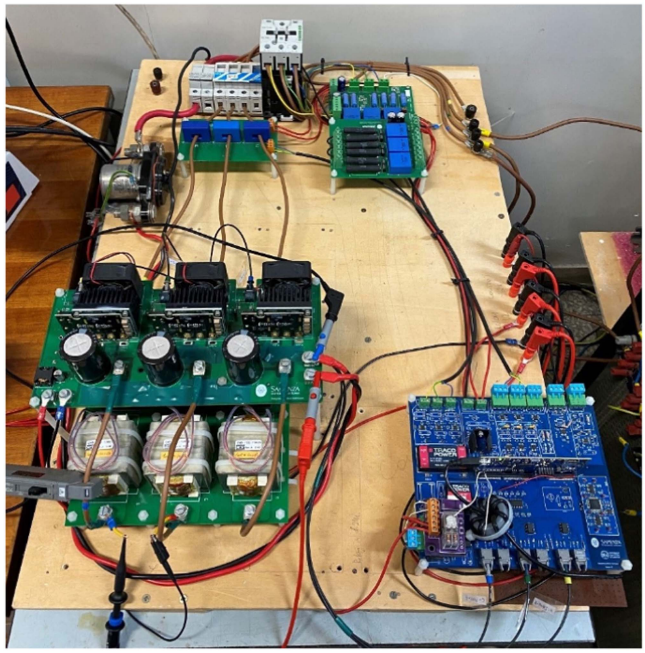

Fig. 7. Experimental setup.

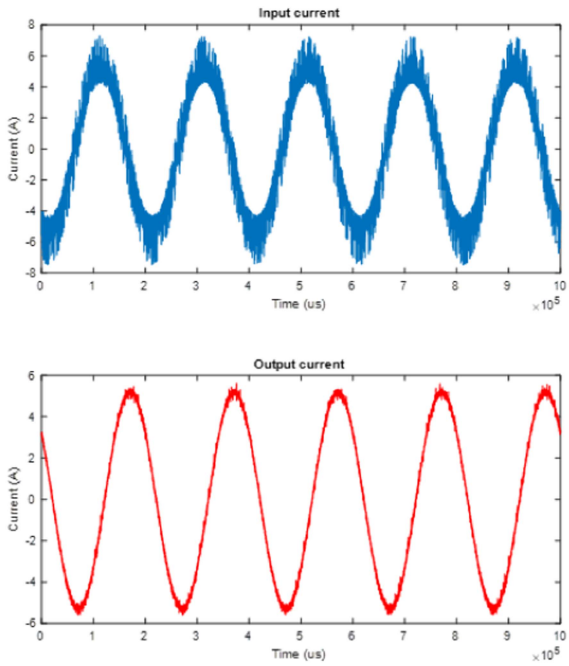

Fig. 8. Input and output currents.

and analyzed here. Figs. 8 and 9 show the *LCL* filter's input and output voltage and current results. The figures illustrate the comparative analysis of input and output electrical characteristics for a power electronic conversion system. The first set of graphs exhibits the input and output currents, where the input current is characterized by a noisy and irregular waveform, indicative of fluctuations that could arise from various factors, such as an unfiltered power supply or a reactive load. The output current,

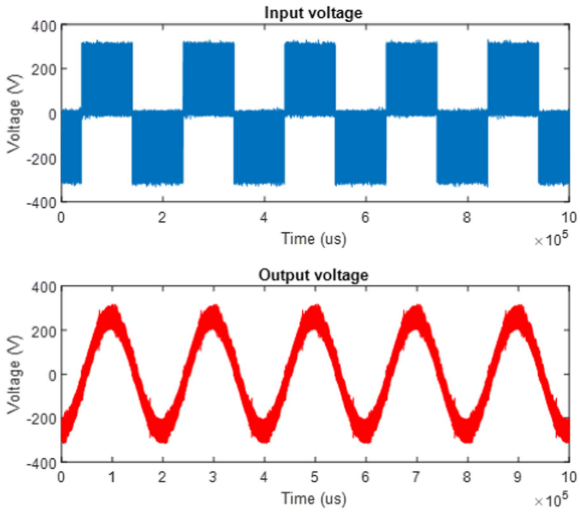

Fig. 9. Input and output voltages.

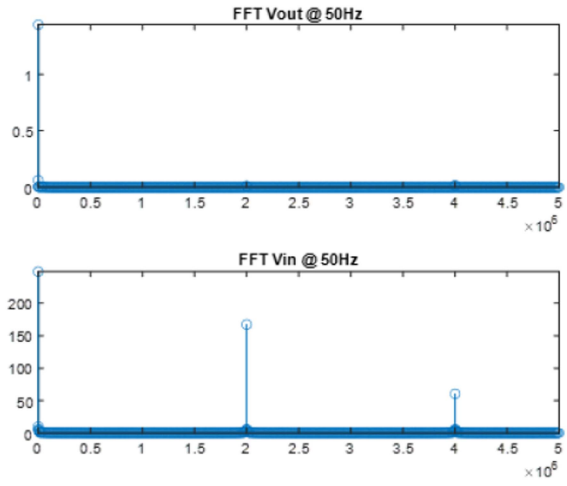

Fig. 10. FFT of input and output voltages.

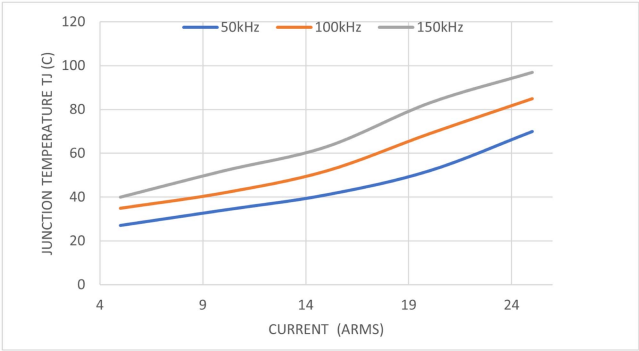

Fig. 11. Junction temperature dependence on current.

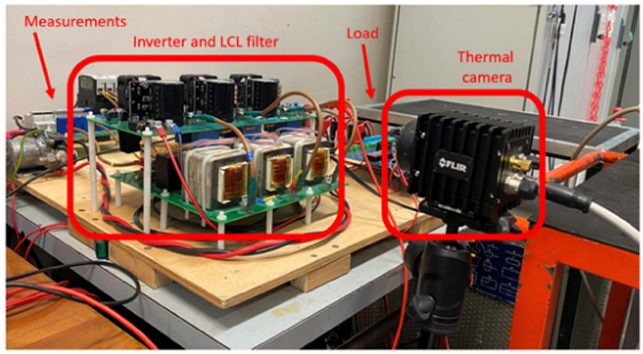

Fig. 12. Thermal test experimental setup.

by contrast, presents a clean and uniform sinusoidal pattern, showcasing the system's efficacy in delivering a smooth and stable alternating current, which is essential for the functionality of downstream electronic devices. The second set of graphs details the voltage profiles. The input voltage displays a square wave commonly associated with digital circuits or pulsewidth modulated signals in power electronics. The sharp transitions between high and low states could also indicate a switched-mode power supply input. The output voltage graph reveals a sine wave conversion consistent with the typical requirements for ac power applications. This transformation is crucial in power systems where a stable and sinusoidal output voltage is necessary, such as grid-tied inverters in renewable energy installations. Together, these figures underscore the system's capabilities to refine and regulate the input electrical signals to meet stringent power quality standards required for sensitive electronic equipment and grid compatibility. The effective filtration and stabilization from the original noisy and square-wave forms to pure sinusoidal indicate sophisticated control mechanisms and power conditioning within the system. Such analyses are vital for advancing power electronic technology, especially in enhancing the integration of renewable energy sources into the existing power infrastructure.

In addition to the waveform analysis, voltage and current frequency spectra were meticulously examined using MATLAB fast Fourier transform (FFT) techniques, with the results depicted in Fig. 10. This figure clearly demonstrates the efficacy of the optimized *LCL* filter in mitigating unwanted frequencies, particularly highlighting that the predominant switching harmonic is centered at 30 kHz, corresponding to the microcontroller's sampling frequency. The system's performance in maintaining power quality is further underscored by the grid current's notably low THD, recorded at just 0.75%. This low THD, closely matching the simulation result of 0.66%, confirms the precision of the simulation models and highlights the robustness of the *LCL* filter design, effectively ensuring high power quality by significantly reducing harmonics.

B. Thermal Analysis

The temperature of GaN switches is measured from temperature monitoring holes. There are four holes located in the center of 4 GaN E-HEMTs to assist with the temperature monitoring during operation. An IR camera Flir A50 (see Fig. 12) is used to monitor the case temperature through these holes. The temperature measured at the center of the GaNPX package will be close to the TJ.

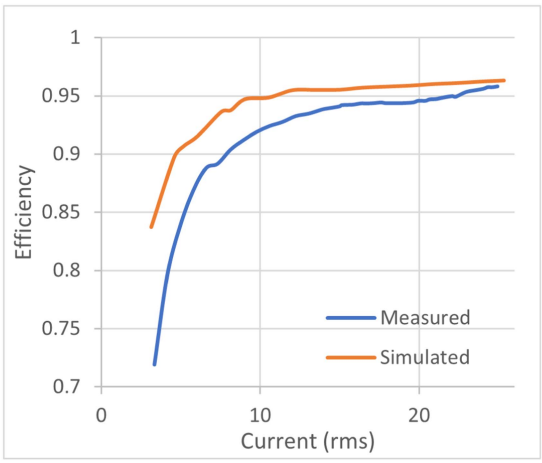

Fig. 13. Efficiency versus current.

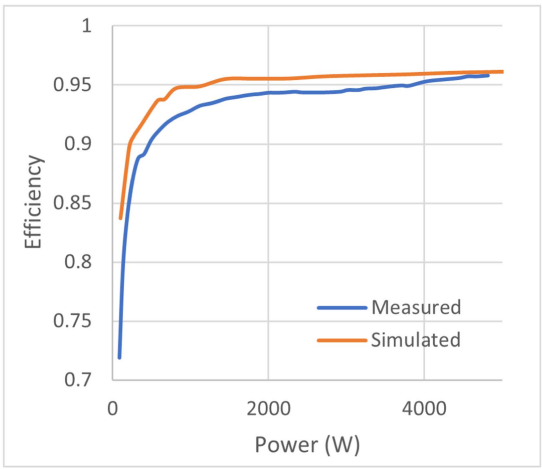

Fig. 14. Efficiency versus power.

Fig. 11 shows the measured junction temperature dependence on rms value of drain current for the different switching frequencies. It can be observed that with the existing switch cooling, the inverter can be safely operated at 20 Arms and 100 kHz. Higher current levels can damage switches unless the improved cooling options are designed and implemented.

Thermal modeling RC thermal models are available in the datasheet to support detailed thermal simulation using SPICE. The thermal models are created using the Cauer model, an RC network model that reflects our devices' real physical properties and packaging structure. By using this approach, the thermal model of their system is extended by adding extra R_θ and C_θ to add IMS and heatsink to the simulation model.

To properly simulate and compare, the thermal resistance and capacitance of the heat sink and IMS board are estimated and added to the thermal circuit. Those thermal parameters mainly depend on material and volume.

C. Efficiency

Figs. 13 and 14 present the efficiency curves of the system operated at 300 V dc and a switching frequency of 100 kHz. These curves compare the measured and simulated efficiencies across varying currents and power levels. A notable observation is that the peak efficiency point is absent from the graph, a consequence attributed to the limitations of the measurement equipment used. However, the data illustrates a convergence between simulation and experimental results at higher power levels. This alignment corroborates the accuracy of the simulation in reflecting the system's performance under substantial loads.

Discrepancies are evident at lower current levels, where the measured efficiency diverges from the simulated values. Such divergence is likely a result of the imperfections inherent in real-world components, which are not fully accounted for in the simulation environment. These imperfections could include factors such as nonideal component behavior, parasitic resistances, and losses that are not present in the idealized models used for simulation.

VII. Conclusion

In conclusion, this article has successfully demonstrated the development and implementation of a three-phase GaN-based inverter, marking a significant step forward in the exploration of GaN technology for PV inverters. Through meticulous experimentation and optimization, this research has confirmed the feasibility of GaN applications in this domain and achieved notable advancements in both reliability and efficiency. One of the key contributions of this work is the demonstration of a GaN-based inverter prototype achieving a competitive peak efficiency of 96%, despite the constraints of the current thermal design and testing equipment, which limited the power range for evaluation. With further optimization of the thermal management system, it is projected that GaN-based inverters could reach efficiencies of 99%, matching or surpassing those of SiC-based systems.

The selected inverter topology, characterized by its simplicity and effectiveness, along with the optimized design of the *LCL* filter for grid-connected applications and the innovative use of fiber optic connections for PWM signal transmission, underscores the potential of GaN technology over conventional Si-based solutions. This article's contribution to the field is significant, as it not only validates the practical viability of GaN FETs in solar applications but also provides a comprehensive framework for the design and optimization of future GaN-based PV inverters.

These accomplishments highlight the transformative potential of GaN technology in renewable energy systems, offering a blueprint for future research and development that promises to elevate the efficiency, reliability, and sustainability of power systems worldwide.

References

[1] J. P. Kozak et al., "Stability, reliability, and robustness of GaN power devices: A review," *IEEE Trans. Power Electron.*, vol. 38, no. 7, pp. 8442–8471, Jul. 2023.

[2] R. Mechouma, B. Azoui, and M. Chaabane, "Three-phase grid connected inverter for photovoltaic systems, a review," in *Proc. 1st Int. Conf. Renewable Energies Veh. Technol.*, 2012, pp. 37–42.

[3] J. Lautner and B. Piepenbreier, "High efficiency three-phase-inverter with 650 v GaN hemts," in *Proc. PCIM Europe Int. Exhib. Conf. Power Electronics, Intell. Motion, Renewable Energy Energy Manage.*, 2016, pp. 1–8.
[4] K. Shirabe et al., "Advantages of high frequency PWM in AC motor drive applications," in *Proc. IEEE Energy Convers. Congr. Expo.*, 2012, pp. 2977–2984.
[5] J. Itoh and T. Araki, "Volume evaluation of a PWM inverter with wide band-gap devices for motor drive system," in *Proc. IEEE ECCE Asia Downunder*, 2013, pp. 372–378.
[6] S. Nagai, Y. Kawai, O. Tabata, S. Choe, N. Negoro, and T. Ueda, "A high-efficient driving isolated drive-by-microwave half-bridge gate driver for a GaN inverter," in *Proc. IEEE Appl. Power Electron. Conf. Expo.*, 2016, pp. 2051–2054.
[7] M. Ugur, H. Saraç, and O. Keysan, "Comparison of inverter topologies suited for integrated modular motor drive applications," in *Proc. IEEE 18th Int. Power Electron. Motion Control Conf.*, 2018, pp. 524–530.
[8] M. Uğur and O. Keysan, "Design of a GaN based integrated modular motor drive," in *Proc. 13th Int. Conf. Elect. Machines*, 2018, pp. 1471–1477.
[9] E. Gurpinar and A. Castellazzi, "SIC and GaN based BSNPC inverter for photovoltaic systems," in *Proc. 17th Eur. Conf. Power Electron. Appl.*, 2015, pp. 1–10.
[10] H. Zhang, B. Ge, Y. Liu, S. Bayhan, R. Balog, and H. Abu-Rub, "Comparison of GaN and sic power devices in application to mw-scale quasi-Z-source cascaded multilevel inverters," in *Proc. IEEE Energy Convers. Congr. Expo.*, 2016, pp. 1–7.
[11] A. Lidow, J. Strydom, M. D. Rooij, and D. Reusch, *GaN Transistors for Efficient Power Conversion*, 2nd ed. New York, NY, USA: Wiley, 2014.
[12] U. K. Mishra, P. Parikh, and Y.-F. Wu, "Algan/GAN HEMTs - an overview of device operation and applications," *Proc. IEEE*, vol. 90, no. 6, pp. 1022–1031, Jun. 2002.
[13] X. Huang, "High frequency GaN characterization and design considerations," Ph.D. dissertation, Center Power Electron. Syst., Blacksburg, VA, USA, 2016. [Online]. Available: https://vtechworks.lib.vt.edu/items/ce73721b-c167-4abf-831a-0ab9b793cd00
[14] C. E. Weitzel et al., "Silicon carbide high-power devices," *IEEE Trans. Electron Devices*, vol. 43, no. 10, pp. 1732–1741, Oct. 1996.
[15] J. A. Cooper, M. R. Melloch, R. Singh, A. Agarwal, and J. W. Palmour, "Status and prospects for SIC power MOSFETs," *IEEE Trans. Electron Devices*, vol. 49, no. 4, pp. 658–664, Apr. 2002.
[16] M. A. Khan, G. Simin, S. G. Pytel, A. Monti, E. Santi, and J. L. Hudgins, "New developments in gallium nitride and the impact on power electronics," in *Proc. IEEE Power Electron. Specialists Conf.*, 2005, pp. 15–26.
[17] B. J. Baliga and M. S. Adler, "Composite circuit for power semiconductor switching," United States Patent and Trademark Office, U.S. Patent No. 4,663,547, 1981. [Online]. Available: https://patents.google.com/patent/US4663547A/en
[18] W. B. Lanford, T. Tanaka, Y. Otoke, and I. Adesida, "Recessed-gate enhancement-mode GaN HEMT with high threshold voltage," *Electron. Lett.*, vol. 41, pp. 449–450, Mar. 2005.
[19] M. Islam, N. Afrin, and S. Mekhilef, "Efficient single phase transformerless inverter for grid-tied PV system with reactive power control," *IEEE Trans. Sustain. Energy*, vol. 7, no. 3, pp. 1205–1215, Jul. 2016.
[20] G. T. Heydt, "The next generation of power distribution systems," *IEEE Trans. Smart Grid*, vol. 1, no. 3, pp. 225–235, Dec. 2010.
[21] Y. A. R. I. Mohamed, "Suppression of low- and high-frequency instabilities and grid-induced disturbances in distributed generation inverters," *IEEE Trans. Power Electron.*, vol. 26, no. 12, pp. 3790–3803, Dec. 2011.
[22] Y. Liu et al., "LCL filter design of a 50-kw 60-khz sic inverter with size and thermal considerations for aerospace applications," *IEEE Trans. Ind. Electron.*, vol. 64, no. 10, pp. 8321–8333, Oct. 2017.
[23] A. Dell'Aquila, M. Liserre, and F. Blaabjerg, "Step-by-step design procedure for a grid-connected three-phase PWM voltage source converter," *Int. J. Electron.*, vol. 91, no. 2, pp. 445–460, 2004.
[24] M. Zabaleta, E. Burguete, D. Madariaga, I. Zubimendi, M. Zubiaga, and I. Larrazabal, "LCL grid filter design of a multimegawatt medium-voltage converter for offshore wind turbine using SHEPWM modulation," *IEEE Trans. Power Electron.*, vol. 31, no. 3, pp. 1993–2001, Mar. 2016.
[25] Z. Wu, M. Aldeen, and S. Saha, "A novel optimisation method for the design of LCL filters for three-phase grid-tied inverters," in *Proc. IEEE Innov. Smart Grid Technol.*, 2016, pp. 214–220.
[26] Y. K. Wu, J. H. Lin, and H. J. Lin, "Standards and guidelines for grid-connected photovoltaic generation systems: A review and comparison," *IEEE Trans. Ind. Appl.*, vol. 53, no. 4, pp. 3205–3216, Jul./Aug. 2017.
[27] T. Basso, S. Chakraborty, A. Hoke, and M. Coddington, "IEEE 1547 standards advancing grid modernization," in *Proc. IEEE Photovolt. Specialist Conf.*, 2015, pp. 1–5.

Orkhan Karimzada (Member, IEEE) was born in Baku, Azerbaijan. He received the B.S. degree in electrical and electronic engineering from the Korea Advanced Institute of Science and Technology (KAIST), Daejeon, South Korea, in 2014, the M.Sc. degree in sustainable energy futures from Imperial College London, London, U.K., in 2016, and the Ph.D. degree in electrical and electronics engineering from Sapienza University of Rome, Rome, Italy, in 2023.

He is currently an Assistant Professor with the School of IT and Engineering, ADA University, Baku, and a Visiting Scholar with George Washington University, Washington, DC, USA. His research interests include power electronics, specifically in the design of power converters using wide-bandgap semiconductors, and their application in renewable energy systems, including electric vehicle charging technologies.

Dr. Karimzada is an active Member of the IEEE Power Electronics Society (PELS) and the IEEE Industry Applications Society (IAS).

Giulio De Donato (Senior Member, IEEE) was born in Cork, Ireland. He received the M.S. and Ph.D. degrees in electrical engineering from Sapienza-University of Rome, Rome, Italy, in 2003 and 2007, respectively.

He is currently an Associate Professor with the Department of Astronautical, Electrical and Energy Engineering (DIAEE), Sapienza-University of Rome. He is Co-PI of a collaborative research agreement between the DIAEE and the Department of Electrical, Electronic Engineering, and Computer Science, University of Catania, Catania, Italy, for research in the field of electric drives. His current research interests include digital control of brushless drives, and analysis and design of permanent magnet machines and of wide-bandgap-semiconductor-based power converters.

Dr. De Donato is a Member of IEEE Industry Applications, IEEE Power Electronics, and IEEE Industrial Electronics Societies. He is a Member of IEEE IAS Industrial Drives Committee, IAS Electric Machines Committee, PELS Technical Committee on Electrical Machines, Drives and Automation, and IES Electrical Machines Committee. He is currently the Vice Chair of the IAS Electric Machines Committee. He was the recipient of the 2014 First Prize Paper Award and of the 2016 Third Prize Paper Award, both from the IAS Industrial Drives Committee. He was acknowledged as an Outstanding Reviewer for IEEE TRANSACTIONS ON POWER ELECTRONICS in 2020 and a Star Reviewer for IEEE TRANSACTIONS ON ENERGY CONVERSION in 2023. He is currently an Associate Editor for IEEE TRANSACTIONS ON INDUSTRY APPLICATIONS and IEEE TRANSACTIONS ON POWER ELECTRONICS.